BULLETIN OF THE POLISH ACADEMY OF SCIENCES
TECHNICAL SCIENCES, Vol. 69(3), 2021, Article number: e137124
DOI: 10.24425/bpasts.2021.137124

Prediction of Kaplan turbine coordination tests based on least squares support vector machine with an improved grey wolf optimization algorithm

Fannie KONG*, Jiahui XIA, Daliang YANG, and Ming LUO

School of Electrical Engineering, Guangxi University, Nanning, 530000, China

Abstract. The optimum combination of blade angle of the runner and guide vane opening with Kaplan turbine can improve the hydroelectric generating the set operation efficiency and the suppression capability of oscillations. Due to time and cost limitations and the complex operation mechanism of the Kaplan turbine, the coordination test data is insufficient, making it challenging to obtain the whole curves at each head under the optimum coordination operation by field tests. The field test data is employed to propose a least-squares support vector machine (LSSVM)-based prediction model for Kaplan turbine coordination tests. Considering the small sample characteristics of the test data of Kaplan turbine coordination, the LSSVM parameters are optimized by an improved grey wolf optimization (IGWO) algorithm with mixed non-linear factors and static weights. The grey wolf optimization (GWO) algorithm has some deficiencies, such as the linear convergence factor, which inaccurately simulates the actual situation, and updating the position indeterminately reflects the absolute leadership of the leader wolf. The IGWO algorithm is employed to overcome the aforementioned problems. The prediction model is simulated to verify the effectiveness of the proposed IGWO-LSSVM. The results show high accuracy with small samples, a 2.59% relative error in coordination tests, and less than 1.85% relative error in non-coordination tests under different heads.

Key words: Kaplan turbine; coordination tests; least squares support vector machine; improved grey wolf optimization.

1. Introduction

Hydropower accounts for a large proportion of the development of renewable energy. It is necessary to keep a hydro turbine in a state of high efficiency to the maximum. The efficiency of the Kaplan turbine is closely related to the coordination relationship of guide vanes and the setting of runner blades. However, the incorrect combination of the coordination relationship leads to a 2% to 8% drop in the unit efficiency, and even the maintenance cycle of the turbine can be shortened by 2 to 3 years. Besides, the optimal combination of coordination relationship can effectively suppress the abnormal vibration of the hydro turbine unit and improve the stability and operating efficiency of the hydroelectric system. Thus, further study is required to obtain the optimal combination of runner blade angle and guide vane opening under various operating conditions.

Many achievements have been attained in the research of Kaplan turbine by scholars. Menarin et al. established the Kaplan turbine dynamic response model, in which the influence of blades to flow rate and efficiency has been considered [1]. Shamsuddeen et al. discovered that installing a fin on the suction side tip of a Kaplan turbine can weaken the leakage cavitation intensity. They simulated unsteady multi-phase cavitation on a numerical Kaplan model on five on-cam conditions [2]. Pennacchi et al. employed vibration measurements for instability detection in the Kaplan turbine [3]. Javadi et al. adopted conventional and non-conventional URANS models to simulate a Kaplan turbine at two operating conditions and successfully captured the flow field structures [4]. However, it is impossible to quickly obtain actual field test results considering the complexity of the turbine model, the long period of data calculation, the model design, and manufacturing [5–10]. A mathematical prediction model should be established to effectively enhance the data and information and find the optimal coordination relationship. Besides, the mathematical model can save a lot of economic and time costs.

The limited hydro turbine test results can be analyzed and processed through the machine learning method, consisting of a neural network, support vector machine, decision tree, and other prediction methods. Quan et al. realized short-term load and wind power forecasting by combining a neural network with lower-upper bound estimation to construct the prediction intervals [11]. Marano et al. employed the dynamic programming (DP) approach to optimize the management of wind and photovoltaic hybrid power plants [12]. Yang et al. utilized a decomposed Newton-Raphson method to solve the nonlinear power equations in unbalanced radial distribution networks [13]. Park et al. adopted sequential convex programming to increase power efficiency by 7.3% in wind farm power production [14]. Ding et al. proposed a constraint relaxation method-based exact penalty function to calculate the optimal power flow [15]. Kebriaei et al. employed the nonsymmetric penalty function to realize short-term load forecasting [16]. Es-

*e-mail: kongfannie@163.com

Manuscript submitted 2021-01-08, revised 2021-03-25, initially accepted for publication 2021-04-02, published in June 2021

eye et al. utilized particle swarm optimization (PSO) to optimize the SVM parameters to achieve short-term photovoltaic solar power prediction based on SCADA and meteorological information [17]. However, PSO suffers from some shortcomings like slow searching speed and low global searching accuracy [18, 19]. Liu et al. employed the regularized extreme learning machine, whose parameters are optimized by grey wolf optimizer (GWO), for the wind speed multistep forecasting [20].

In this paper, an improved grey wolf optimization algorithm (IGWO) is proposed to optimize the least squares support vector machine (LSSVM) regression model to predict the coordination of the Kaplan turbine and non-coordination test data. The prediction results are compared with LSSVM and PSO-LSSVM. By sorting out the prediction results and judging the optimal combination of the coordination relationship, it can guide the parameter setting of the Kaplan turbine.

2. Kaplan turbine coordination relationship

The hydropower unit is mainly composed of a turbine and generator. The electromagnetic moment Me of the generator fluctuates at any time due to the load change. To maintain the unit frequency within the rated range, according to the runner motion equation of the hydropower unit

$$J\frac{\mathrm{d}\omega_t}{\mathrm{d}t} = M_t - M_e\,, \tag{1}$$

where J is the moment of inertia; ω_t is the unit's angular speed, and M_t is the mechanical moment of the turbine. It is necessary to keep the difference of moments constant for realizing the dynamic energy balance. The value of M_t is influenced by adjusting the head H, as shown in (2)

$$M_t = \frac{\rho g Q H \varepsilon}{\omega_t}\,, \tag{2}$$

where ρ is the water density; g is the gravitation acceleration; Q is the flow rate; ε is the turbine efficiency, and the change of guide vane opening a directly affects the value of flow rate. To expand the high-efficiency area of the turbine, a Kaplan turbine was used, which is a double-regulated machine, due to the possibility of adjusting the angle of the runner blades and the guide vanes. As shown in Fig. 1, the high-efficiency zone of the turbine efficiency curve is narrow when the runner blade angle is fixed. However, the Kaplan turbine efficiency curve includes the outer lines of the curves in this set, expanding the high-efficiency zone scope.

The curve of the coordination relationship is an essential basis for adjusting the governor parameters of the Kaplan turbine. When the turbine leaves the factory, the manufacturer provides the coordination curve under different heads. However, these curves are obtained through model turbine tests without considering field factors, such as site reservoir topography and installation links. The coordination and non-coordination tests should be performed to modify the coordination curves and meet the

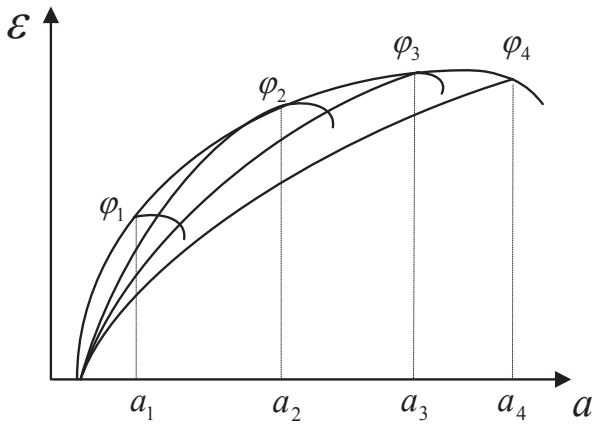

Fig. 1. Efficiency curve of blades

operating requirements of an actual field prototype Kaplan turbine.

The coordination tests refer to the condition under the coordination relationship where the runner blade angle φ and the guide vane opening a have a non-linear one-to-one relationship. These tests are performed when φ and a are not directly related, and their respective values can be adjusted independently, which means that runner blade angle and guide vanes can be adjusted independently during the experiments. The coordination or non-coordination tests are performed under the presence of a constant head H. During the experiments, at first, the runner blade angle φ is kept unchanged. Then the guide vane opening a is gradually changed according to the schedule. Finally, the tests are continued by considering a new fixed value. The difference between coordination and non-coordination tests is that the former are performed using the "Combination unit" [21], while in the latter, the "Combination unit" is removed, as shown in Fig. 2.

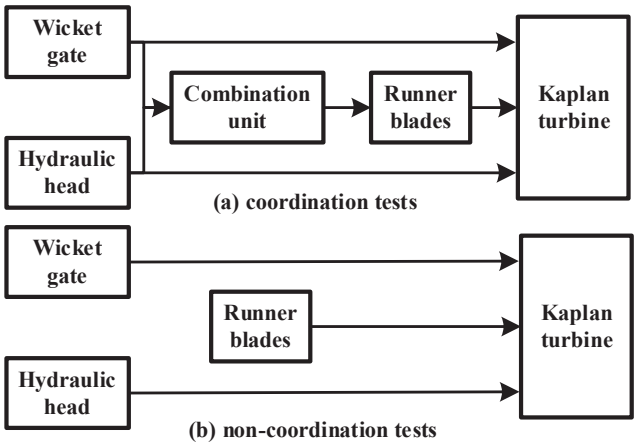

Fig. 2. Explanation of the difference between "coordination tests and non-coordination tests [21]"

Due to the substantial mechanical inertia of the turbine unit, simultaneous adjustment of a and φ in the coordination tests is expensive and time-consuming. Thus, relatively less data is ob-

tained by the coordination tests than the non-coordination ones, which are conducted by adjusting one of these parameters.

By studying the data of the coordination tests of a Kaplan turbine, it is conducive to find the optimal combination of runner blade angle φ and guide vane opening a, to attain the maximum benefit of water energy conversion, ensure that the unit operates in a high-efficiency area, and provide a practical basis for the setting of turbine parameters. Considering the characteristics of Kaplan turbine inputs, this paper employs a hybrid convergence factor and static weight position updating to propose an IGWO algorithm to optimize the LSSVM prediction model.

3. Least squares support vector machine

The LSSVM regression model is based on space vector transformation, where samples are transformed into high-dimensional space by non-linear mapping ψ, and linear regression is constructed in high-dimensional space to realize the original space non-linear relation between input and output, as shown in (3)

$$y(x) = \boldsymbol{\omega}^T \psi(\boldsymbol{x}) + b, \tag{3}$$

where $\boldsymbol{\omega}$ is the normal vector, and b is displacement.

LSSVM regression is to solve the convex quadratic optimal programming problem as presented in [22, 23]

$$\begin{cases} J(\boldsymbol{\omega}, \zeta) = \min\left(\dfrac{1}{2}\|\boldsymbol{\omega}\|^2 + \dfrac{1}{2}\lambda\sum\limits_{k=1}^{n}\zeta_k^2\right), \\ \text{s.t.} \quad y_k = \boldsymbol{\omega}^T\boldsymbol{\psi}(\boldsymbol{x}_k) + b + \zeta_k \quad (k = 1, \ldots, n), \end{cases} \tag{4}$$

where λ is the relative weight; ξ_k is the loss function, and Lagrange multiplier l_k is introduced to construct Lagrange function as

$$L = \frac{1}{2}\boldsymbol{\omega}^T\boldsymbol{\omega} + \frac{1}{2}\lambda\sum_{k=1}^{n}\zeta_k^2 - \sum_{k=1}^{n} l_k\left(\boldsymbol{\omega}^T\boldsymbol{\psi}(\boldsymbol{x}_k) + b + \zeta_k - y_k\right). \tag{5}$$

According to (3), the partial derivatives of $\boldsymbol{\omega}$, ξ_k, b, and l_k are calculated and their values are put to zero, as shown in (6)

$$\frac{\partial L}{\partial \omega_k} = \frac{\partial L}{\partial \zeta_k} = \frac{\partial L}{\partial b} = \frac{\partial L}{\partial l_k} = 0, \tag{6}$$

$$\begin{cases} \boldsymbol{\omega} = \sum\limits_{k=1}^{n} l_k\boldsymbol{\psi}(\boldsymbol{x}_k), \\ l_k = \lambda\zeta_k, \\ \sum\limits_{k=1}^{n} l_k = 0, \\ \boldsymbol{\omega}^T\boldsymbol{\psi}(\boldsymbol{x}_k) + b + \zeta_k - y_k = 0. \end{cases} \tag{7}$$

By eliminating $\boldsymbol{\omega}$ and ξ_k, the problem can be described with the following linear equation

$$\begin{bmatrix} 0 & \boldsymbol{e}^T \\ \boldsymbol{e} & \boldsymbol{K} + \lambda^{-1}\boldsymbol{I} \end{bmatrix}\begin{bmatrix} b \\ \boldsymbol{l} \end{bmatrix} = \begin{bmatrix} 0 \\ \boldsymbol{y} \end{bmatrix}, \tag{8}$$

where $\boldsymbol{K}$ is the n-dimensional matrix of the kernel function; $\boldsymbol{I}$ is the identity matrix, and $\boldsymbol{K}$, $\boldsymbol{e}$, $\boldsymbol{l}$ are defined as follows

$$\begin{cases} \boldsymbol{e} = [1, \cdots, 1]^T, \\ K_{ij} = K(x_i, x_j) = \psi(x_i)^T\psi(x_j), \\ \boldsymbol{l} = [l_1, \cdots, l_n]^T. \end{cases} \tag{9}$$

In this paper, the following Gaussian radial basis function [24] is utilized as kernel function

$$K(x_i, x_j) = \exp\left(-\frac{\|x_i - x_j\|^2}{2\sigma^2}\right), \tag{10}$$

where σ is the kernel coefficient. By considering $\Gamma = \boldsymbol{K} + \lambda^{-1}\boldsymbol{I}$, the solution of (8) can be obtained as

$$\begin{aligned} \begin{bmatrix} b \\ \boldsymbol{l} \end{bmatrix} &= \begin{bmatrix} 0 & \boldsymbol{e}^T \\ \boldsymbol{e} & \Gamma \end{bmatrix}^{-1}\begin{bmatrix} 0 \\ \boldsymbol{y} \end{bmatrix} \\ &= \begin{bmatrix} -\dfrac{1}{\boldsymbol{e}^T\Gamma^{-1}\boldsymbol{e}} & \dfrac{\boldsymbol{e}^T\Gamma^{-1}}{\boldsymbol{e}^T\Gamma^{-1}\boldsymbol{e}} \\ \dfrac{\Gamma^{-1}\boldsymbol{e}}{\boldsymbol{e}^T\Gamma^{-1}\boldsymbol{e}} & \Gamma^{-1}\left(I - \boldsymbol{e}\dfrac{\boldsymbol{e}^T\Gamma^{-1}}{\boldsymbol{e}^T\Gamma^{-1}\boldsymbol{e}}\right) \end{bmatrix}\begin{bmatrix} 0 \\ \boldsymbol{y} \end{bmatrix} \\ &= \begin{bmatrix} \dfrac{\boldsymbol{e}^T\Gamma^{-1}}{\boldsymbol{e}^T\Gamma^{-1}\boldsymbol{e}} \\ \Gamma^{-1}\left(I - \boldsymbol{e}\dfrac{\boldsymbol{e}^T\Gamma^{-1}}{\boldsymbol{e}^T\Gamma^{-1}\boldsymbol{e}}\right) \end{bmatrix}\boldsymbol{y}. \end{aligned} \tag{11}$$

Simplified expressions for $\boldsymbol{l}$ and b are obtained as

$$\begin{bmatrix} b \\ \boldsymbol{l} \end{bmatrix} = \begin{bmatrix} \dfrac{\boldsymbol{e}^T\Gamma^{-1}}{\boldsymbol{e}^T\Gamma^{-1}\boldsymbol{e}}\boldsymbol{y} \\ \Gamma^{-1}(\boldsymbol{y} - \boldsymbol{e}b) \end{bmatrix}. \tag{12}$$

The LSSVM regression function can be described as

$$y(\boldsymbol{x}) = \sum_{k=1}^{n} l_k K(x, x_k) + b. \tag{13}$$

The loss function and the kernel function significantly affect the accuracy of model regression, and their corresponding significant parameters are λ and σ^2. In this paper, the mean squared error (MSE) of the sample is considered as the fitness function, and the IGWO algorithm is utilized to find the optimal values of these parameters.

4. Grey wolf optimizer

GWO as a dynamic population algorithm inspired by the strict hierarchy in the process of searching, following, and hunting was proposed by Mirjalili et al. [25] in 2014.

4.1. Wolf hierarchy. Social levels of grey wolves are shown in Fig. 3. As shown in Fig. 3, there are α, β, γ, and η levels among wolves, and the leadership gradually decreases. α is the

leader wolf, giving general orders to subordinates and leading the wolves to hunt, β assists α in making decisions, γ is subordinate to the decisions of the previous high-level wolf and acts as executive commander for the grass-roots wolf η. The individual level of a wolf changes over time, a new leader wolf can appear among the wolves and social hierarchy turnover may occur. The individual fitness value can describe this situation in the GWO algorithm.

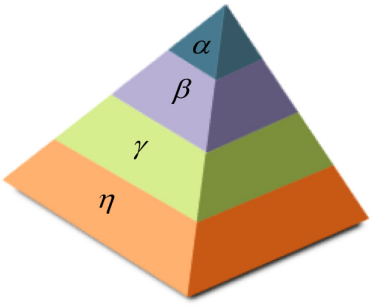

Fig. 3. Social levels of grey wolves

4.2. Wolf hunting. GWO corresponds the social level to the best solution order of the algorithm. This means that the wolf α is the optimal solution, and the wolf β is the sub-optimal solution. The algorithm defines the following updating rules of distance and position between individual an individual wolf and the target

$$\vec{D} = \left|\vec{C} \cdot \vec{X}_O(t) - \vec{X}_W(t)\right|, \tag{14}$$

$$\vec{X}_W(t+1) = \vec{X}_O(t) - \vec{A} \cdot \vec{D}, \tag{15}$$

where $\vec{X}_W$ and $\vec{X}_O$ are the wolf and target positions, respectively; t is the current number of iterations; the vectors $\vec{A}$ and $\vec{C}$ can be calculated as

$$\vec{A} = \vec{\tau} \cdot (2\vec{r}_1 - 1), \tag{16}$$

$$\vec{C} = 2 \cdot \vec{r}_2, \tag{17}$$

$$\vec{\tau} = 2\left(\frac{1-t}{t_{\max}}\right), \tag{18}$$

where $\vec{\tau}$ is the dynamic factor that decays linearly from 2 to 0 with the number of iterations; $\vec{r}_1$ and $\vec{r}_2$ describe the modulus random, where their values are between [0, 1].

When the wolves search for prey, α leads β and γ to track and approach the target prey from different directions. As shown in Fig. 4, the grass-roots wolf η indicates the high-level wolf as the target (analogous to "the prey") and follows the superior wolf to update its position, by the following relations

$$\begin{cases} \vec{D}_\alpha = \left|\vec{C}_1 \cdot \vec{X}_\alpha - \vec{X}_\eta\right|, \\ \vec{D}_\beta = \left|\vec{C}_2 \cdot \vec{X}_\beta - \vec{X}_\eta\right|, \\ \vec{D}_\gamma = \left|\vec{C}_3 \cdot \vec{X}_\gamma - \vec{X}_\eta\right|; \end{cases} \tag{19}$$

$$\begin{cases} \vec{X}_1 = \vec{X}_\alpha - \vec{A}_1 \cdot \vec{D}_\alpha, \\ \vec{X}_2 = \vec{X}_\beta - \vec{A}_2 \cdot \vec{D}_\beta, \\ \vec{X}_3 = \vec{X}_\gamma - \vec{A}_3 \cdot \vec{D}_\gamma, \end{cases} \tag{20}$$

where $\vec{D}_\alpha$, $\vec{D}_\beta$, and $\vec{D}_\gamma$ represent the distances between η and α, β, γ, respectively.

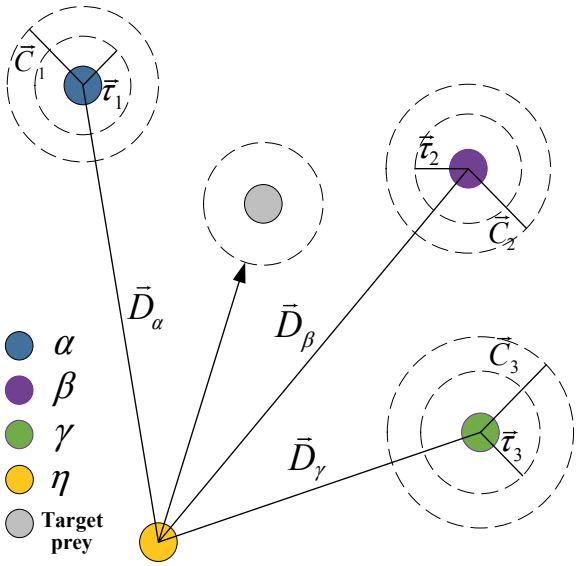

Fig. 4. The diagram of location update in grey wolves

4.3. Attack prey. The convergence factor $\vec{\tau}$ of the GWO algorithm decays linearly with the number of iterations, and according to (16), the value of $\vec{A}$ varies in the range $[-\tau, \tau]$. When $|\vec{A}| > 1$ the grey wolves resign from attacking the current target and turn to search for more suitable prey. Thus, this process expands the global search ability of GWO and avoids a situation when the algorithm falls into the local optimum. In contrast, when $|\vec{A}| \leq 1$, the wolves attack the prey, leading to the local optimum, as shown in Fig. 5. A brief flow chart of the GWO algorithm is presented in Fig. 6.

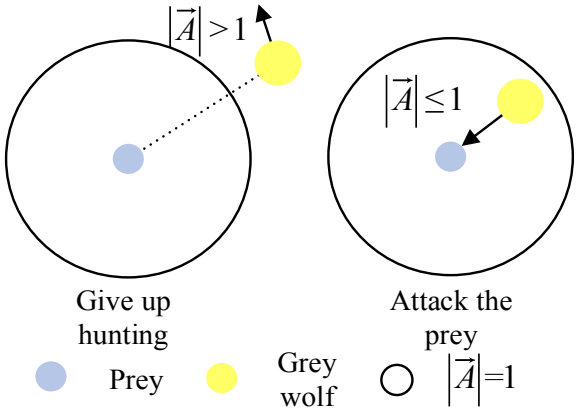

Fig. 5. The hunting selection

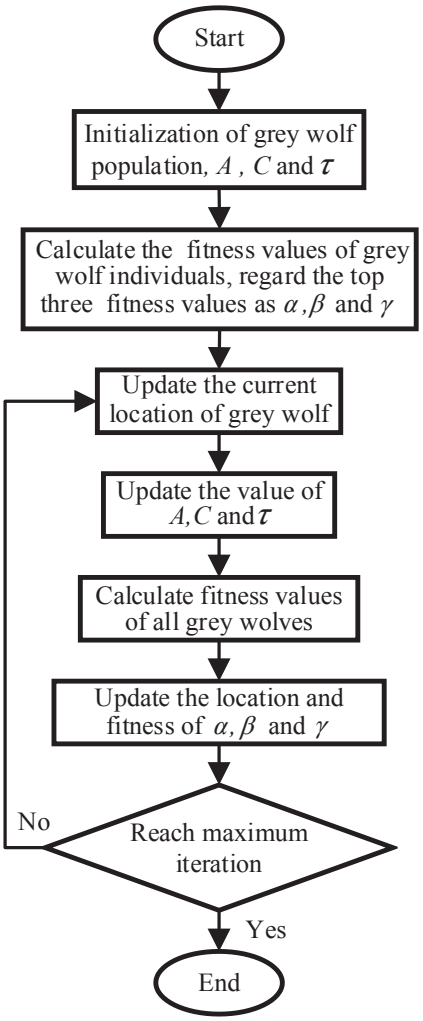

Fig. 6. Flow chart of the GWO

4.4. Improved grey wolf algorithm. Due to the linear decay property of the GWO convergence factor, it is impossible to simulate the actual search process. This paper proposes the following new non-linear convergence factor

$$\vec{\tau}' = \begin{cases} 2 - \dfrac{2t}{t_{\max}}, & t \le \dfrac{t_{\max}}{2}, \\ \dfrac{2}{1+\exp\left[R\left(\dfrac{2t}{t_{\max}} - 1\right)\right]}, & t > \dfrac{t_{\max}}{2}, \end{cases} \tag{21}$$

where $R = 9.903438$. As shown in Fig. 7, the non-linear convergence factor decays too slowly in the early iteration stage, affecting the global search speed of the algorithm. Besides, the decay rate of the linear convergence factor should be improved when calculating the local optimum in the late iteration, which differs from the accelerated attack process by the grey wolf. However, the mixed non-linear convergence factor keeps linear decay in the early stage to improve the global optimization speed. In contrast, it quickly decays in the later stage according to a nonlinear relation and improves the computational efficiency of the local optimization.

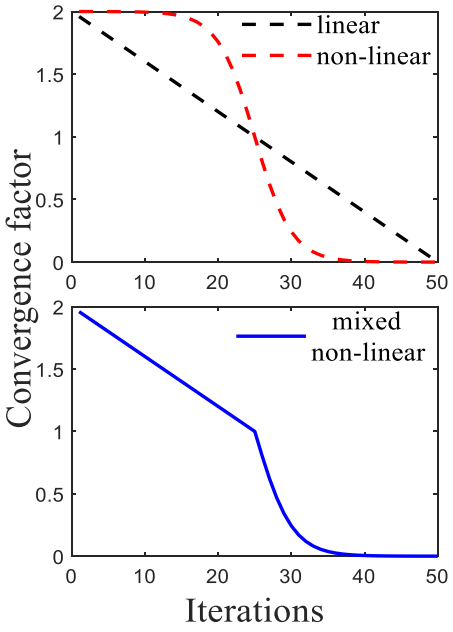

Fig. 7. Factors of mixed nonlinear convergence

In (21), the position weight between grass-roots wolves η and α, β, γ is the same. Taha et al. employed the following modified position updating the formula based on the weighted distance to overcome this problem [26, 27]

$$\begin{cases} \vec{X}_\eta(t+1) = \dfrac{\sum_{i=1}^{3} u_i \vec{X}_i}{\sum_{i=1}^{3} u_i}, \\ u_i = \dfrac{\left|\vec{X}_i\right|}{\sum_{i=1}^{3}\left|\vec{X}_i\right|}. \end{cases} \tag{22}$$

However, this method neglects the absolute leadership of the wolf α, and it should reflect the advantages under the large data condition. Considering the characteristics of the small sample data of the coordination and non-coordination tests, the following static proportional weighting is introduced

$$\vec{X}_\eta(t+1) = \mu_1 \vec{X}_1 + \mu_2 \vec{X}_2 + \mu_3 \vec{X}_3, \tag{23}$$

where μ is the weight of each update direction. In this paper, $\mu_1 = 0.9$, $\mu_2 = 0.06$, $\mu_3 = 0.04$ are considered. The simulation results demonstrate that the static weight is more suitable than the weighted distance under the condition of small samples of the Kaplan turbine.

5. Simulation analysis

The data set is divided into training and prediction sets to simulate the actual prediction, as shown in Table 1. The training set includes the input runner blade angle φ, guide vane open-

ing a, and Kaplan turbine output power P, which are provided to IGWO-LSSVM for learning. Only φ and a are considered in the prediction set, and the trained IGWO-LSSVM regression model gives the prediction value. The prediction results are compared with backpropagation (BP) neural network, LSSVM, PSO-LSSVM, and GWO-LSSVM methods [28–31] to evaluate the effectiveness of the proposed model. To ensure the generalization of the model, a k-fold cross-validation approach is employed, and $k = 3$ is chosen.

Table 1
Data of working with coordination tests

Training set				Prediction set		
No.	φ	a	P	No.	φ	A
1	44.2	6.62	3226.52	11	69.3	36.3
2	85.5	69.4	13466.38	12	78.3	52.4
3	88.4	77.0	14368.31	13	92.7	81.5
⋮	⋮	⋮	⋮	14	49.6	12.4
9	50.2	13.1	4388.89	15	93.0	87.0
10	60.0	23.8	6467.69	16	89.5	80.5

5.1. Prediction of coordination tests. The coordination test data are acquired from a hydropower station in Guangxi, China, and the test head $H = 6.0$ m. The first above 65% of the data is utilized for training, and the last above 35% is utilized for testing. The optimization parameters of each algorithm are shown in Table 2. The hyperparameters of each algorithm are presented in Table 3. Considering the limited number of samples, the swarm size is chosen as 3, the number of iterations is considered 50, the PSO inertia factor is selected as 0.4, and PSO acceleration factors $c_1 = 1.4$, and $c_2 = 1.1$. Since the data samples in this paper are not normalized, the LSSVM parameters have large values; the λ optimization range is [8.038e4, 9.7435e6], while the σ^2 search interval is [30, 206].

Table 2
Parameters of the optimization algorithms

Algorithm	Parameter		
	λ	σ^2	Iteration number
PSO	2.0590e6	30.1	50
GWO	5.7902e6	30.01	50
IGWO	9.7435e6	30.01	50

Table 3
Hyperparameters of each algorithm

Algorithm	Parameter			
	Swarm size	Inertia factor	c_1	c_2
PSO	3	0.4	1.4	1.1
GWO	3			
IGWO	3			

The prediction effect of each method is shown in Fig. 8. Besides, the root mean square error (RMSE), relative error (RE), and mean absolute error (MAE) are chosen as evaluation indices of the prediction, as shown in Table 4.

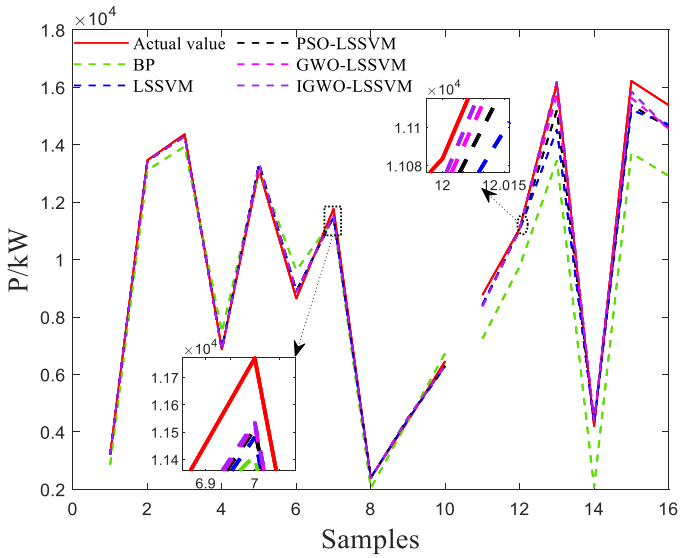

Fig. 8. Effective diagram of prediction with coordination tests

Table 4
Evaluation indices of the prediction of coordination tests

Meethod	Indicator		
	RMSE	RE	MAE
BP	2163.286	17.56%	2101.60
LSSVM	828.657	5.20%	622.39
PSO-LSSVM	621.457	4.28%	512.50
GWO-LSSVM	467.491	3.23%	386.82
IGWO-LSSVM	413.454	2.59%	310.25

Since the input is small sample data, the BP neural network learning degree is insufficient, and its error is significant. LSSVM can guarantee relatively general prediction accuracy under the small sample condition. Compared with GWO and PSO algorithms, the prediction accuracy of IGWO-LSSVM is significantly improved to 2.59%.

5.2. Prediction of non-coordination tests. The multi-head non-coordination tests data are collected from a hydropower station in Guangxi, China, in which its corresponding set heads are $H = 4.1$ m, $H = 5.0$ m, and $H = 6$ m, respectively. The first above 80% of the data are employed for training, and the last above 20% are employed for the testing. These data are as shown in Table 5.

Table 5
Data of working with non-coordination tests

$H = 4.1$ m							$H = 5$ m							$H = 6$ m						
Training set				Prediction set			Training set				Prediction set			Training set				Prediction set		
No.	φ	a	P	No.	φ	a	No.	φ	a	P	No.	φ	a	No.	φ	a	P	No.	φ	a
1	9.69	50.9	1893.04	21	26.8	62.0	1	50.0	76.1	8451.27	21	74.9	90.3	1	80.8	90	15473.77	26	23	63.4
2	38.7	78.0	5520.28	22	38.7	82.0	2	30.5	77.7	6026.65	22	20.1	51.7	2	13.6	42.2	4074.97	27	69	79.1
⋮	⋮	⋮	⋮	23	16.5	67.9	⋮	⋮	⋮	⋮	23	20.1	64.5	⋮	⋮	⋮	⋮	28	35.5	62.5
19	16.5	51.9	2550.00	24	38.7	86.0	19	74.9	86.3	10667.59	24	30.5	70.1	24	80.8	84.3	15031.14	29	80.8	91.4
20	9.69	58.8	1949.61	25	26.8	66.0	20	9.27	58.7	2783.74	25	30.5	74.5	25	35.5	75.3	8678.40	30	13.6	56.4

Table 6
Evaluation indices of prediction with non-coordination tests

Test head	$H = 4.1$ m			$H = 5$ m			$H = 6$ m		
Indicator Method	RMSE	RE	MAE	RMSE	RE	MAE	RMSE	RE	MAE
BP	824.27	15.92%	686.01	1292.82	18.73%	1192.15	380.42	3.52%	332.64
LSSVM	166.57	3.14%	135.43	221.05	2.84%	180.70	287.06	2.28%	214.88
PSO-LSSVM	139.12	2.69%	115.92	156.82	1.81%	115.07	245.46	1.99%	188.02
GWO-LSSVM	101.91	2.03%	87.47	119.61	1.51%	96.30	210.25	1.67%	157.28
IGWO-LSSVM	90.48	1.83%	79.03	110.88	1.48%	94.79	193.51	1.51%	142.41

The prediction effect of non-coordination tests is shown in Figs. 9–11, while the best fitting to the actual value is obtained by the IGWO-LSSVM algorithm. The evaluation indices show that the proposed IGWO-LSSVM prediction model can still maintain high accuracy in the multi-head condition, as shown in Table 6.

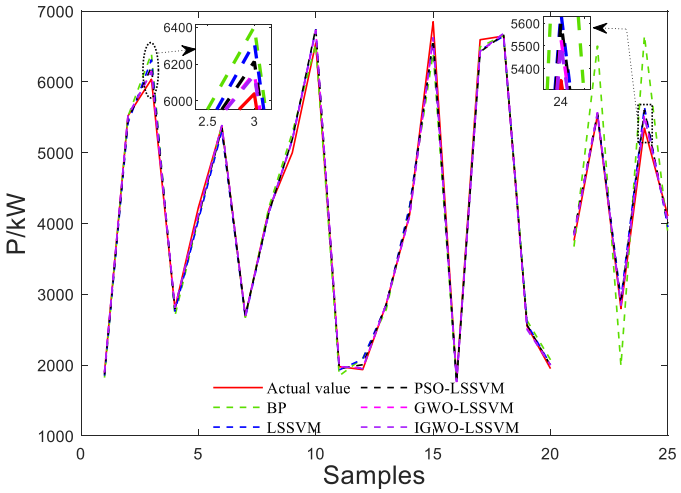

Fig. 9. Effective diagram of prediction with non-coordination tests for $H = 4.1$ m

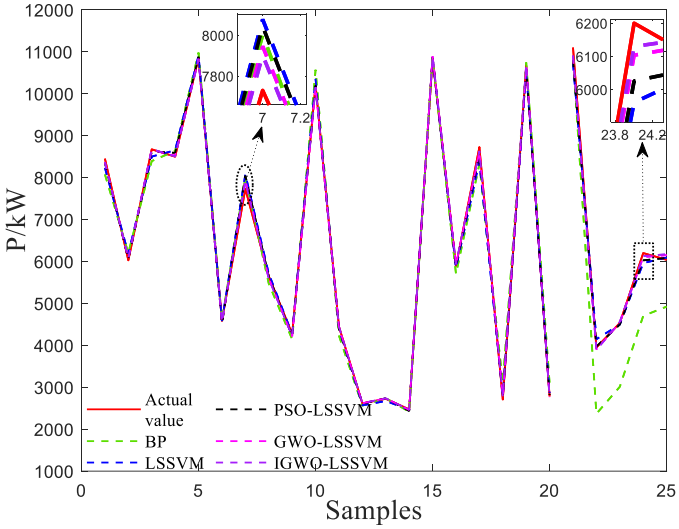

Fig. 10. Effective diagram of prediction with non-coordination tests for $H = 5$ m

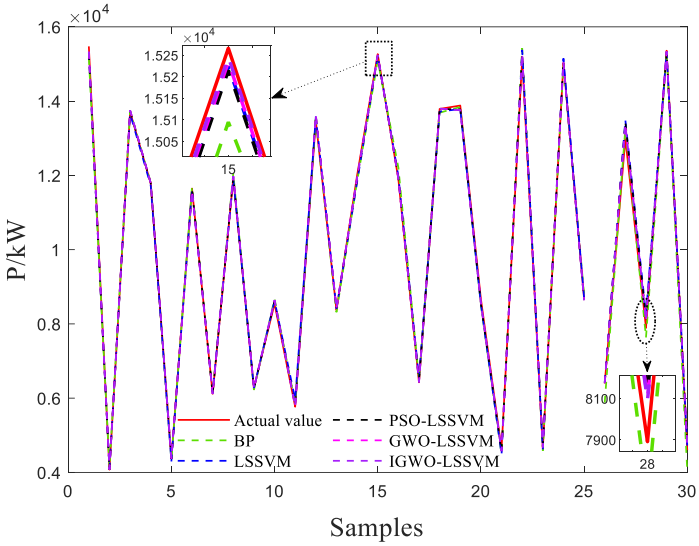

Fig. 11. Effective diagram of prediction with non-coordination tests for H = 6 m

6. Conclusions

The coordination tests of the prototype Kaplan turbine are time-consuming and expensive, and the obtained test data are scarce, making it impossible to guide the optimal parameters setting of hydropower unit equipment in an all-around way.

This paper proposes an IGWO-LSSVM prediction model to save test costs and increase the amount of data. Considering the Kaplan turbine test characteristics of small samples, the IGWO employs static proportional weights and a new non-linear convergence factor. MSE is utilized as a fitness function to optimize the prediction results by iteration several times, while RMSE and MAE evaluation indices are utilized to evaluate the prediction effect. A multi-method forecasting comparison study is performed by combining BP neural network, LSSVM, PSO-LSSVM, and GWO-LSSVM algorithms under the conditions of turbine coordination tests and multi-head non-coordination tests to verify the feasibility of the proposed method. The obtained results confirm the advantages of the IGWO-LSSVM model, including the fast convergence and high accuracy, by considering multi-static head coordination characteristics of the turbine under the condition of small samples. In coordination tests, compared with the PSO-LSSVM and GWO-LSSVM algorithms, the prediction effects of IGWO-LSSVM are improved above 39.49% and 19.81%, respectively. While in non-coordination tests, the improvement is above 24.77% and 7.14%, averagely.

In the next step, the impact of external disturbances on the mathematical prediction model will be analyzed by combining the environmental factors such as reservoir topography and pipeline layout of the hydropower station.

Acknowledgements. National Natural Science Foundation of China, Grant NO.51167003; Guangxi Natural Science Foundation, grant 2014 GXNSFAA118320.

References

[1] H.A. Menarin, H.A. Costa, G.L.M. Fredo, R.P. Gosmann, E.C. Finardi, and L.A. Weiss, "Dynamic Modeling of Kaplan Turbines Including Flow Rate and Efficiency Static Characteristics", *IEEE Trans. Power Syst.* 34(4), 3026–3034 (2019).

[2] M.M. Shamsuddeen, J. Park, Y. Choi, and J. Kim, "Unsteady multi-phase cavitation analysis on the effect of anti-cavity fin installed on a Kaplan turbine runner", *Renew. Energy* 162, 861–876 (2020).

[3] P. Pennacchi, P. Borghesani, and S. Chatterton, "A cyclostationary multi-domain analysis of fluid instability in Kaplan turbines", *Mech. Syst. Signal Process.* 60–61, 375–390 (2015).

[4] A. Javadi and H. Nilsson, "Detailed numerical investigation of a Kaplan turbine with rotor-stator interaction using turbulence-resolving simulations", *Int. J. Heat Fluid Flow* 63, 1–13 (2017).

[5] D. Kranjcic and G. Štumberger, "Differential Evolution-Based Identification of the Nonlinear Kaplan Turbine Model", *IEEE Trans. Energy Convert.* 29(1), 178–187 (2014).

[6] Z. Krzemianowski, "Engineering design of low-head Kaplan hydraulic turbine blades using the inverse problem method", *Bull. Pol. Acad. Sci. tech. Sci*. 67(6), 1133–1147 (2019).

[7] A.B. Janjua, M.S. Khalil, M. Saeed, F.S. Butt, and A.W. Badar, "Static and dynamic computational analysis of Kaplan turbine runner by varying blade profile", *Energy Sustain. Dev.* 58, 90–99 (2020).

[8] Y. Wu, S. Liu, H. Dou, S. Wu, and T. Chen, "Numerical prediction and similarity study of pressure fluctuation in a prototype Kaplan turbine and the model turbine", *Comput. Fluids* 56, 128–142 (2012).

[9] S.J. Daniels, A.A.M. Rahat, G.R. Tabor, J.E. Fieldsend, and R.M. Everson, "Shape optimisation of the sharp-heeled Kaplan draft tube: Performance evaluation using Computational Fluid Dynamics", *Renew. Energy*. 160, 112–126 (2020).

[10] F. Thiery, R. Gustavsson, and J.O. Aidanpää, "Dynamics of a misaligned Kaplan turbine with blade-to-stator contacts", *Int. J. Mech. Sci*. 99, 251–261 (2015).

[11] H. Quan, D. Srinivasan, and A. Khosravi, "Short-Term Load and Wind Power Forecasting Using Neural Network-Based Prediction Intervals", *IEEE Trans. Neural Netw. Learn. Syst.* 25(2), 303–315 (2014).

[12] V. Marano, G. Rizzo, and F.A. Tiano, "Application of dynamic programming to the optimal management of a hybrid power plant with wind turbines, photovoltaic panels and compressed air energy storage", *Appl. Energy*. 97, 849–859 (2012).

[13] N. Yang and H.Chen, "Decomposed Newton algorithm-based three-phase power-flow for unbalanced radial distribution networks with distributed energy resources and electric vehicle demands", *Int. J. Electr. Power Energy Syst.* 96, 473–483 (2018).

[14] J. Park and K.H. Law, "Layout optimization for maximizing wind farm power production using sequential convex programming", *Appl. Energy*. 151, 320–334 (2015).

[15] T. Ding, R. Bo, F. Li, Y. Gu, Q. Guo, and H. Sun, "Exact Penalty Function Based Constraint Relaxation Method for Optimal Power Flow Considering Wind Generation Uncertainty", *IEEE Trans. Power Syst*. 30(3), 1546–1547 (2015).

[16] H. Kebriaei, B.N. Araabi, and A. Rahimi-Kian, "Short-Term Load Forecasting With a New Nonsymmetric Penalty Function", *IEEE IEEE Trans. Power Syst*. 26 (4), 1817–1825 (2011).

[17] A.T. Eseye, J. Zhang, and D. Zheng, " Short-term photovoltaic solar power forecasting using a hybrid Wavelet-PSO-SVM model based on SCADA and Meteorological information", *Renew. Energy*. 118, 357–367 (2018).

[18] Y. Li and X. Wnag, "Improved dolphin swarm optimization algorithm based on information entropy", *Bull. Pol. Acad. Sci. Tech. Sci.* 67(4), 679–685 (2019).

[19] H. Koyuncu and R. Ceylan, "A PSO based approach: Scout particle swarm algorithm for continuous global optimization problems", *J. Comput. Des. Eng.* 6, 129–142 (2019).

[20] H. Liu, H.P. Wu, Y.F. Li, "Smart wind speed forecasting using EWT decomposition, GWO evolutionary optimization, RELM learning and IEWT reconstruction", *Energy Conv. Manag.* 161, 266–283 (2018).

[21] M. Gratza, R. Witzmann, Ch.J. Steinhart, M. Finkel, M. Becker, T. Nagel, T. Wopperer, and H. Wackerl, "Frequency Stability in Island Networks: Development of Kaplan Turbine Model and Control of Dynamics", in *2018 Power Systems Computation Conference (PSCC)*, Dublin, Ireland, 2018, pp. 1–7, doi: 10.23919/PSCC.2018.8442445.

[22] M. Malvoni, M.G. D. Giorgi, and P.M. Congedo, "Photovoltaic forecast based on hybrid PCA–LSSVM using dimensionality reducted data", *Neurocomputing* 211, 72–83 (2016).

[23] Y. Sun, Y. Liu, and H. Liu, "Temperature Compensation for a Six-Axis Force/Torque Sensor Based on the Particle Swarm Optimization Least Square Support Vector Machine for Space Manipulator", *IEEE Sensors Journal*. 16(3), 798–805 (2016).

[24] X. Yan and N.A. Chowdhury, "Mid-term electricity market clearing price forecasting: A hybrid LSSVM and ARMAX approach", *Int. J. Electr. Power Energy Syst.* 53, 20–26 (2013)

[25] S. Mirjalili, S.M. Mirjalili, and A. Lewis, "Grey Wolf Optimizer", *Adv. Eng. Softw.* 69, 46–61 (2014).

[26] I.B.M. Taha and E.E. Elattar, "Optimal reactive power resources sizing for power system operations enhancement based on improved grey wolf optimiser", *IET Gener. Transm. Distrib.* 12(14), 3421–3434 (2018).

[27] W. Long, J.J. Jiao, X.M. Liang, and M.Z. Tang, "Inspired grey wolf optimizer for solving large-scale function optimization problems", *Appl. Math. Model.* 60, 112–126 (2018).

[28] Y. Li, B. Zhang, and X. Xu, "Decoupling control for permanent magnet in-wheel motor using internal model control based on back-propagation neural network inverse system", *Bull. Pol. Acad. Sci. Tech. Sci.* 66(6), 961–972 (2018).

[29] D. Huang, S. He, X. He, and X. Zhu, "Prediction of wind loads on high-rise building using a BP neural network combined with POD", J. Wind Eng. Ind. Aerodyn. 170, 1–17 (2017).

[30] A.L. Yang, W.D. Li, and X. Yang, "Short-term electricity load forecasting based on feature selection and Least Squares Support Vector Machines", *Knowledge-Based Syst*. 163, 159–173 (2019).

[31] N.A. Menad, Z. Noureddine, A. Hemmati-Sarapardeh, and S. Shamshirband, "Modeling temperature-based oil-water relative permeability by integrating advanced intelligent models with grey wolf optimization: Application to thermal enhanced oil recovery processes", *Fuel* 242, 649–663 (2019).